Research article

Fangjie Shu, Xuefeng Jiang, Guangming Zhao and Lan Yang*

A scatterer-assisted whispering-gallery-mode microprobe

https://doi.org/10.1515/nanoph-2018-0063
Received May 18, 2018; revised June 15, 2018; accepted June 18, 2018

Abstract: A fiber-based whispering-gallery-mode (WGM) microprobe, combining both the high optical field enhancement of the WGMs and the compact structure of the optical fiber, is highly desired for sensing and imaging. Here we report a WGM microsphere resonator coupled to a single-mode fiber interfaced by a graded-index lens. By scattering a focused laser beam through a nano-scatterer, with the help of a two-step focusing technique as well as Purcell effects, the efficient far-field coupling of WGMs with an efficiency as high as 16.8% has been demonstrated in our system. With the feature of both input and output of the probe light propagating along the same fiber, such a scatterer-assisted WGM microprobe will serve as a convenient tool for sensing/imaging applications.

Keywords: fiber optics sensors; microcavities; sensors.

1 Introduction

Whispering-gallery-mode (WGM) microresonators have attracted increasing attention in the last two decades in the fields of microlaser [1–5], optomechanics [6–9], bio/chemical/thermal sensing [10–18], nonlinear optics [19–24], and so on [25], due to their ultrahigh-quality (Q) factors and small-mode volumes. It is critical to effectively couple light into and out of the microresonator for the aforementioned experiments and applications. Traditionally, a near-field coupler, for example, an integrated waveguide or a tapered fiber, within the evanescent field of a resonant mode, is used to couple light into and out of the WGM microresonator [26, 27]. However, the evanescent-field coupling method essentially requires not only a strict phase-matching condition [28] but also a high-resolution lithography to define the wavelength-scale waveguide-resonator gap or a high-precision alignment of the fiber taper. Another approach is to tailor the cavity geometry to achieve a directional output [29–32]; following time-reversal symmetry, the cavity modes can be excited by a free-space laser beam [4, 33–39]. Although some excellent designs have produced a unidirectional emission with a relatively small divergence angle and achieved the efficient free-space coupling, the coupling efficiency is much lower than the near-field coupler, especially for the ultrahigh-Q factor modes [34]. Besides, each cavity material (refractive index) requires a particular cavity shape design, making it inconvenient to operate.

Recently, another coupling method has been proposed and demonstrated to exploit an extra defect/scatterer placed inside the mode field to couple a free-space laser beam into resonant modes [40–43]. This coupling method is free from the phase-matching condition and suitable for resonators with different materials. However, a practical coupling scheme utilizing the compact scatterer-assisted coupling scheme with a high coupling efficiency still remains to be demonstrated. Here in this paper, for the first time we experimentally realized an efficient far-field light coupling between a conventional single-mode optical fiber and high-Q WGMs via a scatterer placed on the surface of a microsphere resonator. Both input and output lights are transmitted along the same optical fiber. Specifically, a fiber nanotip mounted on a 3-axis nano-stage is utilized as a light scatterer, so we could adjust its position on the resonator in the experiments. A graded-index (GRIN) lens coupled with a single-mode fiber is used to focus the laser beam of 1550 nm wavelength band onto the nanotip, which then scatters the focused laser into WGMs with a coupling efficiency as high as 16.8%. Particularly, the reflection signal is also collected by the same GRIN lens and fiber, making the whole coupling system a fiber-based WGM microprobe, which will become a compact platform for sensing/imaging applications.

***Corresponding author: Lan Yang,** Department of Electrical and Systems Engineering, Washington University in St. Louis, One Brookings Drive, St. Louis, Missouri 63130, USA, e-mail: yang@seas.wustl.edu
Fangjie Shu: Department of Physics, Shangqiu Normal University, Shangqiu, Henan 476000, P.R. China; and Department of Electrical and Systems Engineering, Washington University in St. Louis, St. Louis, Missouri 63130, USA
Xuefeng Jiang and Guangming Zhao: Department of Electrical and Systems Engineering, Washington University in St. Louis, St. Louis, Missouri 63130, USA

2 Theories and experiments

2.1 The coupling process and the spectrum

The experimental setup is illustrated in Figure 1A. A microsphere resonator with a diameter of 35 μm and a fiber nanotip with a diameter of around 0.2 μm at the very top of the cone shape [44] are used in the experiments. The probe laser in 1550 nm band is first coupled into a fiber and then focused onto the surface of the microsphere by a GRIN lens with a working distance of 200 μm. Different from the traditional focusing method, here we develop a special two-step focusing technique. Specifically, the focused laser with a beam size of around 6 μm is further focused by the microsphere itself onto the nanotip located at the back surface of the microsphere. Most of the light scattered by the nanotip is coupled into the resonant mode with the help of the Purcell effect when the incident light is scanned across a WGM. Meanwhile, the cavity-mode field can also be coupled out of the cavity by the same nanotip in the reversed optical path and then collected by the same GRIN lens and fiber. Finally, the collected reflection signal is routed by a circulator and detected by a photodetector, which is connected with an oscilloscope to monitor the reflection spectrum of the resonant system. In the experiments, three 3-axis nano-stages are used to control the relative positions of the microsphere, the nanotip, and the incident laser beam to optimize the coupling condition.

A typical reflection spectrum is shown as the black curve in Figure 1B. As a comparison, the red curve in Figure 1B shows the reflection spectrum of the same mode with the nanotip removed from the surface of the microsphere, in which the resonant peaks disappear subsequently. Therefore, we conclude that the resonant peaks are caused by the Rayleigh scattering of the nanotip. Note that the doublet peak indicates a clear mode splitting, which is caused by the mode coupling of the clockwise (CW) and counter-clockwise (CCW) modes induced by the scattering of the nanotip [11]. It further proves the role of the nanotip in the Rayleigh scattering. In other words, the nanotip in the coupling system not only couples light into and out of WGMs of the microsphere but also enables mode coupling between the CW and CCW modes. Moreover, this coupling mechanism is free from the phase-matching condition and applies to all the modes in the microsphere. As shown in Figure 1C, there are five spikes in the reflection spectrum (red curve), showing the same

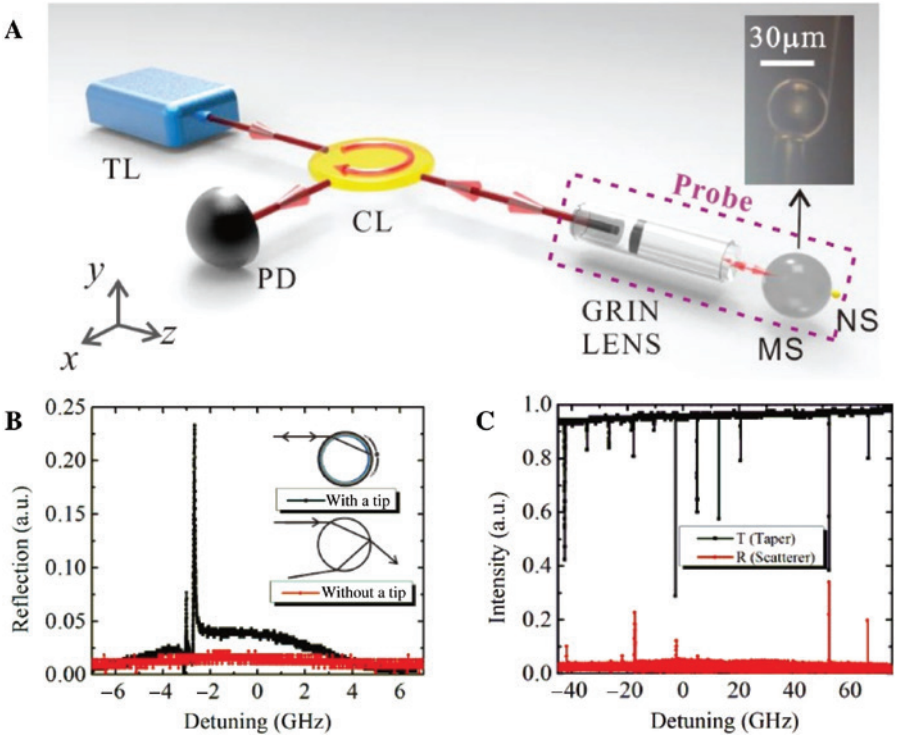

Figure 1: (A) Illustration of the experimental setup.
TL, tunable laser; PD, photo-detector; CL, circulator; GRIN LENS, graded-index lens; MS, microsphere; NS, nano-scatterer. Inset: optical image of a microsphere approached by a fiber nanotip in the experiment. (B) Reflection spectra with (black) and without (red) a nanotip. (C) Optical spectra of a microsphere resonator with the scatterer-assisted coupling (red) and the fiber taper coupling (black).

frequencies with resonant dips in the transmission spectrum (black curve), which is obtained by a traditional fiber taper coupling method. It is worth noting that some modes are not excited by the nanotip, which can be attributed to the mismatching between the mode distributions and the location of the nanotip.

An overall coupling efficiency of 2.8% is derived from the measured peak power of the reflection signal divided by the input probe power. It should be noted that the overall coupling efficiency includes both the input and the output coupling processes, which are two reversible processes and thus should have similar coupling efficiency. Therefore, the approximate coupling efficiency of the proposed coupling method is the square root of the overall coupling efficiency, that is, 16.8%. The high scattering-based coupling efficiency is attributed to both Purcell effect and the proposed two-step focusing technique.

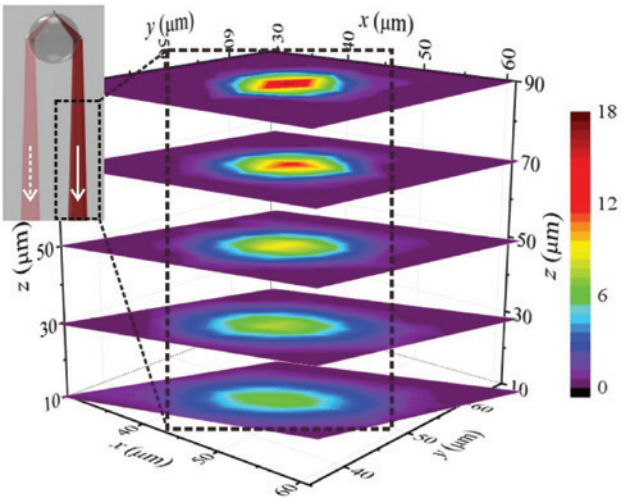

Figure 2: Nanotip-induced emission pattern measured at different positions from the resonator.
Inset: sketch illustrating the light emission from the microsphere resonator to free space.

2.2 The coupling efficiencies as a function of the positions of the lens

The free-space coupling efficiency is typically determined by the matching between the resonant emission pattern and the incident probe laser beam [33], which is affected by the alignment between the microsphere and the GRIN lens in our design. In our experiments, a GRIN lens with a working distance of around 200 μm is utilized to focus the probe laser beam down to around 6 μm. The divergence angle of the focused beam is about 3.27°. To measure the divergence angle of the nanotip-induced scattering pattern, we excite the resonant mode by a tapered fiber and measure the three-dimensional scattering pattern collected by the GRIN lens, which is mounted on a 3-axis nano-stage. By fitting the focused profile of the emission pattern from the resonator as shown in Figure 2, we find a divergence angle of 4.18°, which is similar to the divergence angle of the incoming beam to the resonator. By adjusting the position of the GRIN lens that provides incident light to the microsphere resonator, we could optimize the overlap between the free-space light beam and scatterer-induced scattering pattern to improve the coupling efficiency. Note that the GRIN lens also collects the scattering pattern.

To study the dependence of the coupling efficiencies on the relative position of the lens to the resonator, we mount the GRIN lens, the microsphere, and the nanotip on three 3-axis nano-stages, respectively. By moving the GRIN lens solely, we investigate how the coupling efficiencies of a WGM with Q factor around 5.6×10^6 vary with the positions of the lens, which affect both the incident light and the collected light from the resonator (Figure 3). The coordinate system is defined in Figure 1A. The maximum reflection intensities, which indicate the coupling efficiencies, as a function of the relative x and y between the probe laser beam and the microsphere are shown in Figure 3A and B, respectively. Reflection peaks are observed when adjusting both x and y positions of the GRIN lens. The widths of the peaks are 3.2 and 7.1 μm for the relative x and y, respectively. In other words, the coupling system has a position tolerance of about 2–4 times of the wavelength in the lateral plane. Note that the y-related width is more than two times of that in the x direction, because here the scatterer is a nanotip with a larger dimension in the y direction than in the x direction. Different from x and y positions, there is a periodic oscillation of the reflection signal with varied z position, as shown in Figure 3C. The period of the oscillation is about 0.77 μm, which is the half of the probe light wavelength. This oscillation stems from the interference between the reflected light from the end-face of the GRIN lens and the resonant emission from the microsphere. The average reflection signal decreases less than 20% in a range of 10 μm, showing a very large position tolerance in the z direction. It is worth noting that the x-related curve is asymmetric in Figure 3A, which is attributed to the non-resonant reflection by the microsphere. Specifically, at position A, where the input light aims at the center of the microsphere, the non-resonant reflection of the probe light by the microsphere can be collected by the coupling lens, and then forms a high reflection background, as shown in the frequency-scanning curve

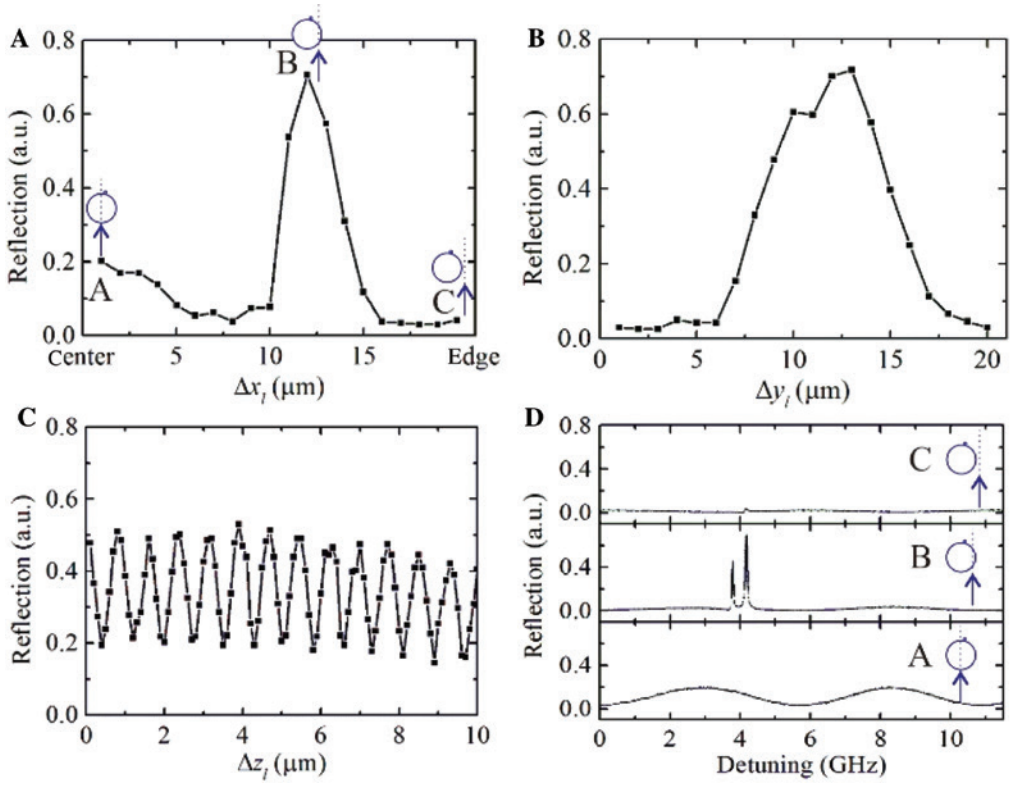

Figure 3: The amplitude of the reflection as a function of the spatial position of the GRIN lens (incident beam).
Peaks in the reflection spectra vary with the relative position Δx_l (A), Δy_l (B), and Δz_l (C) of the GRIN lens (incident beam) when keeping the nanotip-sphere coupling system invariant. (D) Reflection spectra at three positions of Δx_l. The letters A, B and C in (A) and (D) represent three cases of relative position Δx_l between the incident beam (arrows in the schematic diagram beside the letters) and the microsphere.

in Figure 3D. On the other hand, at position C, where the probe beam is far away from the microsphere, neither resonant nor non-resonant light can be reflected.

2.3 The coupling efficiencies as a function of the positions of the nanotip and the microsphere

In this section, we investigate the coupling efficiencies varying with the relative positions of the nanotip on the equator of the microsphere. The experiment is performed by moving both the nanotip and the microsphere in the *x* axis with the incident laser beam focused. More specifically, the microsphere moves with a step of 2 μm. For every position of the microsphere, we move the nanotip along the equator of the microsphere in the *x*-*z* plane continuously and record both the top-view imaging by a CCD camera and the reflection spectrum with a frame rate of ~3 Hz (see Visualization 1, a composite video at $\Delta_{x_s} = -11$ μm).

The position of the nanotip on the microsphere is characterized by a polar coordinate, θ, in the *x*-*z* plane, as defined in the left inset of Figure 4A. Specifically, when the nanotip is near or on the equator of the microsphere, a light spot caused by the resonant scattering of a illumination light can be imaged in the top view, which can help to mark the position of the nanotip, θ. Meanwhile, the reflection signal, which is proportional to the coupling efficiency of every nanotip position, is acquired by the photodetector. Figure 4A shows the reflection as a function of the nanotip position with the microsphere fixed at $\Delta x_s = -11$ μm, where a main peak accompanied with several side lobes is presented. The width of the main peak is about 3° corresponding to 0.9 μm along the equator of the microsphere. A 2D simulation of a Gaussian beam focused by a microsphere explains the fringes. The simulated field distribution around the rim of the microsphere is shown in the right inset of Figure 4A, where several fringes can be clearly seen on the surface of the microsphere. Note that the size of the nanotip (~0.2 μm) is much smaller than the period of the fringes (~1 μm). Thus the fringes can be resolved by the nanotip moving along the ring of the spherical resonator. In addition, the fluctuation of the coupling efficiency maps the distribution of the intensity of the focused field, which further verifies that the resonant coupling is caused by the nanotip.

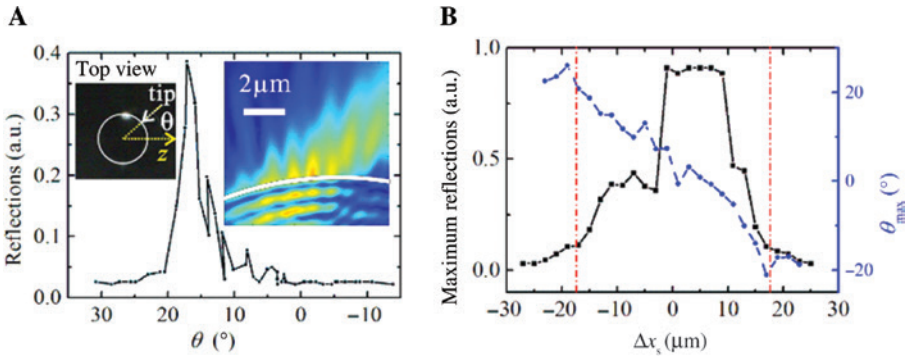

Figure 4: The amplitude of the reflection as a function of the spatial position of the microsphere and the nanotip.
(A) Peak value of the reflection varies with the position of the nanotip on the sphere with the microsphere fixed at $\Delta x_s = -11$ μm. Left inset: top view of the sphere-tip coupling system. The white arrow points out the scattering spot of the nanotip. Right inset: simulated distribution of a Gaussian beam focused by the microsphere. (B) Maximum peak value in the reflection spectrum (black solid curve) and the corresponding position of the nanotip (blue dashed curve) vary with the position of the sphere, Δx_s, when the incident beam is fixed. The vertical red dot-dashed lines indicate the boundaries of the microsphere at $\Delta x_s = 0$ μm.

In the experiment, for every position of the microsphere, the maximum reflection and the corresponding azimuth angle θ_{max} are recorded, as shown in the black and blue curves in Figure 4B, respectively. The two vertical red dot-dashed lines in Figure 4B mark the two boundaries of the microsphere. A relatively high coupling efficiency can be achieved in a large range of ~15 μm, in which most of the incident Gaussian beam illuminates on the microsphere. It is worth noting that the reflection curve deviates from the mirror symmetry relative to the center of the microsphere ($\Delta x_s \sim 0$). This deviation may be attributed to the misalignment between the incident Gaussian beam and the z axis. The azimuth angle θ_{max} shows an approximately linear relationship with Δx_s (blue curve in Figure 4B). The results show the critical role of the two-step focusing technique that requires alignment of the GRIN lens and the microsphere resonator as well as the position of the scatterer to effectively couple light in and out of a high-Q WGM resonator through a single-mode optical fiber.

3 Conclusion

To summarize, we have demonstrated a compact scheme to efficiently couple light in and out of a high-Q WGM resonator to form a fiber-based microprobe. The incident laser beam is focused by the microsphere itself as well as the GRIN lens, which is also used to collect the resonant reflection signal. With the help of the Purcell effect and the two-step focusing technique, the excitation efficiency of a high-Q factor WGM as high as 16.8% has been achieved. The proposed coupling method is robust to the mechanical vibration between the microsphere and the incident probe beam. Both the probe light and the reflection resonant signal are guided by the same single-mode fiber, making the whole coupling system an excellent fiber-based WGM microprobe for a variety of applications, including lasing, sensing, and imaging. By packaging the microsphere, the nanotip, the GRIN lens, and the fiber together with low-refractive-index glue [24] in the future, the WGM microprobe will open up a new direction for a variety of sensing/imaging applications, such as nanoparticle/biomolecule sensing, resonant acoustic imaging, and *in situ* monitoring of dynamic chemical reactions.

Acknowledgments: This work was supported by the National Science Foundation (EFMA1641109); The Army Research Office (W911NF1210026 and W911NF1710189); The Key Science and Technology Program of Henan Province, China (182102410070); The State Scholarship Fund from China Scholarship Council (201508410405); The Program for Innovative Research Team (in Science and Technology) in University of Henan Province (16IRTSTHN028); The Open Project of Key Laboratory of Quantum Information (KQI201502). We thank L. Xu, S. H. Huang, W. Chen, and C.-L. Zou for discussions.

References

[1] Yang L, Vahala KJ. Gain functionalization of silica microresonators. Opt Lett 2003;28:592–4.
[2] Yang L, Armani DK, Vahala KJ. Fiber-coupled erbium microlasers on a chip. Appl Phys Lett 2003;83:825–6.
[3] He L, Özdemir ŞK, Yang L. Whispering gallery microcavity lasers. Laser Photon Rev 2013;7:60–82.

[4] Jiang XF, Xiao YF, Zou CL, et al. Highly unidirectional emission and ultralow-threshold lasing from on-chip ultrahigh-Q microcavities. Adv Mate 2012;24:OP260–4.
[5] Jiang XF, Zou CL, Wang L, Gong Q, Xiao YF. Whispering-gallery microcavities with unidirectional laser emission. Laser Photon Rev 2016;10:40–61.
[6] Aspelmeyer M, Kippenberg TJ, Marquardt F. Cavity optomechanics. Rev Mod Phys 2014;86:1391–452.
[7] Monifi F, Zhang J, Özdemir ŞK, et al. Optomechanically induced stochastic resonance and chaos transfer between optical fields. Nat Photonics 2016;10:399–405.
[8] Jiang X, Wang M, Kuzyk MC, et al. Chip-based silica microspheres for cavity optomechanics. Opt Express 2015;23:27260–5.
[9] Chen X, Liu YC, Peng P, Zhi Y, Xiao YF. Cooling of macroscopic mechanical resonators in hybrid atom-optomechanical systems. Phys Rev A 2015;92:033841.
[10] Vollmer F, Braun D, Libchaber A, et al. Protein detection by optical shift of a resonant microcavity. Appl Phys Lett 2002;80:4057–9.
[11] Zhu J, Özdemir ŞK, Xiao YF, et al. On-chip single nanoparticle detection and sizing by mode splitting in an ultrahigh-Q microresonator. Nat Photonics 2010;4:46–9.
[12] Shao L, Jiang XF, Yu XC, et al. Detection of single nanoparticles and lentiviruses using microcavity resonance broadening. Adv Mater 2013;25:5616–20.
[13] Dantham VR, Holler S, Barbre C, et al. Label-free detection of single protein using a nanoplasmonic-photonic hybrid microcavity. Nano Lett 2013;13:3347–51.
[14] Zhi Y, Yu XC, Gong Q, Yang L, Xiao YF. Single nanoparticle detection using optical microcavities. Adv Mater 2017;29:1604920.
[15] Huang SH, Sheth S, Jain E, et al. Whispering gallery mode resonator sensor for in situ measurements of hydrogel gelation. Opt Express 2018;26:51–62.
[16] Li BB, Wang QY, Xiao YF, et al. On chip, high-sensitivity thermal sensor based on high-Q polydimethylsiloxane-coated microresonator. Appl Phys Lett 2010;96:251109.
[17] Xu X, Jiang X, Zhao G, Yang L. Phone-sized whispering-gallery microresonator sensing system. Opt Express 2016;24:25905–10.
[18] Xu L, Jiang X, Zhao G. High-Q silk fibroin whispering gallery microresonator. Opt Express 2016;24:20825–30.
[19] Spillane SM, Kippenberg TJ, Vahala KJ. Ultralow-threshold Raman laser using a spherical dielectric microcavity. Nature 2002;415:621–3.
[20] Kippenberg TJ, Holzwarth R, Diddams SA. Microresonator-based optical frequency combs. Science 2011;332:555–9.
[21] Yang L, Carmon T, Min B, Spillane SM, Vahala KJ. Erbium-doped and Raman microlasers on a silicon chip fabricated by the sol-gel process. Appl Phys Lett 2005;86:1–3.
[22] Jiang XF, Xiao YF, Yang QF, et al. Free-space coupled, ultralow-threshold Raman lasing from a silica microcavity. Appl Phys Lett 2013;103:101102.
[23] Yang Y, Jiang X, Kasumie S, et al. Four-wave mixing parametric oscillation and frequency comb generation at visible wavelengths in a silica microbubble resonator. Opt Lett 2016;41:5266.
[24] Zhao G, Ozdemir ŞK, Wang T, et al. Raman lasing and Fano lineshapes in a packaged fiber-coupled whispering-gallery-mode microresonator. Science Bulletin 2017;62;875–8.
[25] Xiao YF, Gong Q. Optical microcavity: from fundamental physics to functional photonics devices. Science Bulletin 2016;61;185–6.
[26] Hagness SC, Rafizadeh D, Ho ST, Taflove A. FDTD microcavity simulations: design and experimental realization of waveguide-coupled single-mode ring and whispering-gallery-mode disk resonators. J Lightwave Technol 1997;15:2154–65.
[27] Cai M, Painter O, Vahala KJ. Observation of critical coupling in a fiber taper to silica-microsphere whispering gallery mode system. Phys Rev Lett 2000;85:74–7.
[28] Knight JC, Cheung G, Jacques F, Birks TA. Phase-matched excitation of whispering-gallery-mode resonances by a fiber taper. Opt Lett 1997;22:1129.
[29] Nöckel JU, Stone AD. Ray and wave chaos in asymmetric resonant optical cavities. Nature 1997;385:45–7.
[30] Wiersig J, Hentschel M. Combining directional light output and ultralow loss in deformed microdisks. Phys Rev Lett 2008;100:033901.
[31] Zou CL, Sun FW, Dong CH, et al. High-Q and unidirectional emission whispering gallery modes: principles and design. IEEE J Sel Top Quantum 2013;19:9000406.
[32] Shu FJ, Zou CL, Sun FW. An optimization method of asymmetric resonant cavities for unidirectional emission. J Lightwave Technol 2013;31:2994–8.
[33] Zou CL, Shu FJ, Sun FW, et al. Theory of free space coupling to high-Q whispering gallery modes. Opt Express 2013;21: 9982–95.
[34] Shao L, Wang L, Xiong W, et al. Ultrahigh-Q, largely deformed microcavities coupled by a free-space laser beam. Appl Phys Lett 2013;103:121102.
[35] Liu ZP, Jiang XF, Li Y, et al. High-Q asymmetric polymer microcavities directly fabricated by two-photon polymerization. Appl Phys Lett 2013;102:221108.
[36] Yang QF, Jiang XF, Cui YL, Shao L, Xiao YF. Dynamical tunneling-assisted coupling of high-Q deformed microcavities using a free-space beam. Phys Rev A 2013;88:023810.
[37] Shu FJ, Zou CL, Sun FW. Dynamic process of free space excitation of asymmetric resonant microcavity. J Lightwave Technol 2013;31:1884–9.
[38] Jiang X, Shao L, Zhang SX, et al. Chaos-assisted broadband momentum transformation in optical microresonators. Science 2017;358:344–7.
[39] Zhang SX, Wang L, Li ZY, et al. Free-space coupling efficiency in a high-Q deformed optical microcavity. Opt Lett 2016;41: 4437–40.
[40] Liu YC, Xiao YF, Jiang XF, et al. Cavity-QED treatment of scattering-induced free-space excitation and collection in high-Q whispering-gallery microcavities. Phys Rev A 2012;85:013843.
[41] Song Q, Cao H. Highly directional output from long-lived resonances in optical microcavity. Opt Lett 2011;36:103–5.
[42] Zhu J, Özdemir ŞK, Yilmaz H, et al. Interfacing whispering-gallery microresonators and free space light with cavity enhanced Rayleigh scattering. Sci Rep 2014;4:6396.
[43] Aveline DC, Baumgartel LM, Lin G, Yu N. Whispering gallery mode resonators augmented with engraved diffraction gratings. Opt Lett 2013;38:284–6.
[44] Zhu J, Özdemir SK, He L, Yang L. Controlled manipulation of mode splitting in an optical microcavity by two Rayleigh scatterers. Opt Express 2010;18:23535–43.

Supplementary Material: The online version of this article offers supplementary material (https://doi.org/10.1515/nanoph-2018-0063).